ORIGINAL RESEARCH

3D-QSAR of p38-α mitogen-activated protein kinase inhibitors: pyridopyridazin-6-ones (part 1)

Sujit G Bhansali
Vithal M Kulkarni

Department of Pharmaceutical Chemistry, Poona College of Pharmacy, Bharati Vidyapeeth Deemed University, Pune, Maharashtra, India

→ Video abstract

Point your SmartPhone at the code above. If you have a QR code reader the video abstract will appear. Or use: http://dvpr.es/1ab8E0q

Correspondence: Vithal M Kulkarni
Department of Pharmaceutical Chemistry, Poona College of Pharmacy, Bharati Vidyapeeth Deemed University, Paud Road, Erandwane, Pune-411 038, Maharashtra, India
Tel +91 98 9080 2623
Fax +91 20 2543 9383
Email vmkulkarni60@gmail.com

Abstract: p38-α mitogen-activated protein kinase (MAPK) is considered to be a novel target for the development of new anti-inflammatory agents. Inhibitors of this enzyme can provide new therapeutics for the treatment of various inflammatory diseases, such as rheumatoid arthritis, Crohn's disease, and inflammatory bowel disease. Three-dimensional quantitative structure-activity relationship (3D-QSAR) studies for pyridopyridazin-6-ones exhibiting p38-α MAPK inhibition were performed using comparative molecular field analysis (CoMFA) and comparative molecular similarity indices analysis (CoMSIA). The study included 70 compounds. The QSAR model was generated using a training set of 45 compounds. The energy-minimized structure of the most active compound in the series, compound 70, was used as a template for alignment, which was done with an aligned database. The optimum partial least squares analysis model on CoMFA and CoMSIA descriptors showed "leave-one-out" cross-validation correlation coefficients (q^2) of 0.611 and 0.493, and non-cross-validated correlation coefficients (r^2_{ncv}) of 0.973 and 0.815, respectively. The statistical quality of the generated model was further analyzed by bootstrapping analysis and by more robust cross-validation testing using cross-validation by two groups (leave-half-out method) to check the internal reliability within the dataset. The predictive ability of the generated CoMFA and CoMSIA model was analyzed by an external test set of 25 compounds, resulting in predictive correlation coefficients (r^2_{pred}) of 0.630 and 0.403, respectively. The generated model may provide useful guidance for future synthesis of potent p38-α MAPK inhibitors.

Keywords: three-dimensional quantitative structure-activity relationship, comparative molecular field analysis, comparative molecular similarity indices analysis, p38-α MAPK

Introduction

Inflammation is a complex biological process associated with an exaggerated human immune system response involving various activated immune cells and biomolecules. There has been a new realization about the role of inflammation in a wide variety of diseases, including cancer. While acute inflammation is a part of the defense response, chronic inflammation can lead to cancer, arthritis, diabetes, and cardiovascular, pulmonary, and neurologic disease.[1] p38-α mitogen-activated protein kinase (MAPK) is a serine-threonine kinase activated by environmental stimuli, including tumor necrosis factor-α, interleukin-1β, and stress. Excessive production of tumor necrosis factor-α and interleukin-1β may lead to various diseases, such as rheumatoid arthritis, psoriasis, and inflammatory bowel disease.[2–5]

In 2000, 5-(2,6-dichlorophenyl)-2-(2,4-difluorophenylthio)-6H-pyrimido [1,6-b] pyridazin-6-one (VX-745) was discovered and found to have a high level of activity against

a broad spectrum of kinases.[6] Since then, many compounds have been discovered and are undergoing clinical trials for inflammatory conditions.[7] Hence, p38-α MAPK may be a novel target for development of new anti-inflammatory agents.

A series of pyridopyridazin-6-ones with potent and selective inhibition activity toward p38-α MAPK have been reported.[8,9] In order to derive a correlation between the structure and biological activity of these inhibitors, we carried out a three-dimensional quantitative structure-activity relationship (3D-QSAR) study using comparative molecular field analysis (CoMFA)[10] and comparative molecular similarity indices analysis (CoMSIA).[11] The CoMFA method is applicable to a set of compounds showing biological activity with a similar mechanism of action. Steric and electrostatic interaction energies were calculated between each part of the molecule and a probe atom, usually an sp3 carbon atom with a +1.0 charge at lattice intersection points.[12]

One of the advantages of CoMFA is its ability to predict the biological activity of molecules and represent the relationship between steric and electrostatic properties and biological activity in the form of contour maps. In CoMSIA, a probe atom is used to calculate similarity indices, at regularly spaced grid points for the prealigned molecules. The advantage of CoMSIA over CoMFA is that no singularities occur at the atomic positions because the fields are evaluated using a Gaussian function and therefore no arbitrary definitions of cutoff limits are used.[11] Partial least squares (PLS) analysis is used to calculate cross-validated r^2 (r^2_{cv}) and conventional r^2 values.

In this paper, 3D-QSAR CoMFA and CoMSIA methods were applied to generate quantitative models to predict the activity of pyridopyridazin-6-ones and to specify regions in space where interactive fields might enhance their activity. The predictive ability of the generated model was validated by an external validation technique using test set compounds. The obtained model was further used to generate contour maps for explaining the interaction of these compounds and to study the structure-activity relationship.

Materials and methods
Dataset
Details of the compounds used for the present study are taken from the literature.[8,9] These molecules have been reported as inhibitors of the p38-α MAPK enzyme. The pyridopyridazin-6-ones were grouped into a training set of 45 compounds and a test set of 25 compounds. Selection of training set and test set molecules was done randomly among the series. The training set was used to generate 3D-QSAR

models, and the test set was used to validate the quality of the model. All biological activities used in the present study were expressed as:

$$pIC_{50} = -\log_{10} IC_{50} \qquad (1)$$

where pIC_{50} is the predicted nanomolar concentration of the inhibitor producing 50% inhibition. In all the models subsequently developed, pIC_{50} values were used as the dependent variable. pIC_{50} is usually given in terms of molar concentration (mol/L, or M). Therefore, to obtain a pIC_{50}, an IC_{50} should be specified in units of M. When IC_{50} is expressed in μM or nM, it needs to be converted to M before conversion to pIC_{50}. The computation of $pIC_{50} = \log 1/IC_{50} = -\log IC_{50}$ is presented below:

Step 1. Consider IC_{50} value of compound 1 which is in nanomolar concentration

Step 2. IC_{50} value is 7 nmol/L = 7×10^{-9} mol/L

Step 3. Compute $pIC_{50} = -\log IC_{50} = -(\log 7 \times 10^{-9}) = -(-8.155) = 8.155$

Similarly, the pIC_{50} values of other compounds are calculated. Structures and related inhibitory activities are shown in Table 1.

Molecular modeling and alignment
The molecular modeling studies were carried out using SYBYL-X 2.0 (Tripos Associates Inc, St Louis, MO, USA).[13] Three-dimensional structures of all compounds were drawn using the Sketch module and were charged using the Gasteiger-Huckel method. Energy minimization was performed using a standard Tripos molecular mechanics force field with 10,000 iterations.[14] Molecular alignment is the most important part of 3D-QSAR analysis. In the present study, structures of 1–70 compounds were aligned using a common fragment by the align database for generation of best CoMFA and CoMSIA models. Compound 70 was selected as a template because it is the most potent derivative in the series. The fragment used as the template for aligning is shown in Figure 1. The aligned database of molecules is shown in Figure 2.
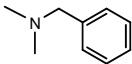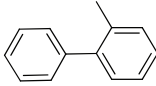
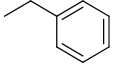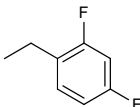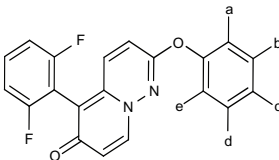## Calculation of CoMFA and CoMSIA fields
To calculate the CoMFA and CoMSIA fields, a three-dimensional cubic lattice was defined automatically with grid spacing of 2 Å and extending to 4 Å units beyond all the aligned molecules in all the three axes (X, Y, Z directions). An sp³ carbon atom bearing a +1 charge and having a radius of 1.52 A° was used as a probe atom. The

Table 1 p38-α MAPK inhibitory activity of 7-substituted quinolizin-2-ones (1–7) and pyridopyridazin-6-ones (8–70) used for training and test sets
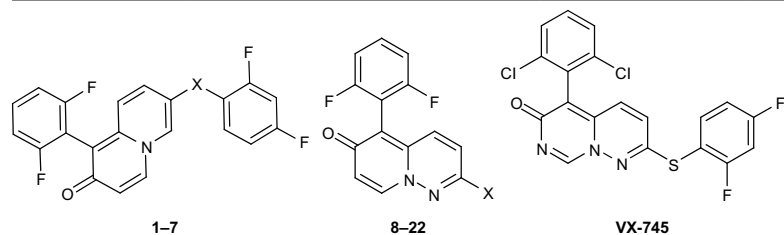
Compound number	X	p38α IC$_{50}$ (nm)	pIC$_{50}$
1*	–	7	8.155
2*	S	320	6.495
3*	O	190	6.721
4*	CH$_2$	93	7.032
5*	NHCH$_2$	870	6.060
6*	C$_2$H$_2$	890	6.051
7*	C$_2$H$_4$	490	6.310
8*		3.2	8.495
9*		720	6.143
10		4.7	8.328
11*		10,000	5.000
12		1,300	5.886
13		160	6.796
14		10,000	5.000
15*		1,300	5.886
16		719	6.143
17		3.5	8.456
18		20	7.699

(*Continued*)

Table 1 (*Continued*)

Compound number	X	p38α IC$_{50}$ (nm)	pIC$_{50}$
19		650	6.187
20		480	6.319
21*		1,430	5.845
22		7.6	8.119
23–52			

Compound number	A	B	C	D	E	p38α IC$_{50}$ (nm)	pIC$_{50}$
23*	F	–	–	–	–	12	7.921
24*	Cl	–	–	–	–	44	7.357
25	CH$_3$	–	–	–	–	92	7.036
26*	OCH$_3$	–	–	–	–	82	7.086
27	CF$_3$	–	–	–	–	2,400	5.620
28	–	F	–	–	–	420	6.377
29	–	Cl	–	–	–	240	6.620
30	–	CH$_3$	–	–	–	70	7.155
31	–	OCH$_3$	–	–	–	10,000	5.000
32	–	CF$_3$	–	–	–	10,000	5.000
33	–	–	F	–	–	48	7.319
34*	–	–	Cl	–	–	79	7.102
35	–	–	CH$_3$	–	–	260	6.585
36	–	–	OCH$_3$	–	–	10,000	5.000
37	–	–	CF$_3$	–	–	10,000	5.000
38	F	F	–	–	–	32	7.495
39*	Cl	Cl	–	–	–	32	7.495
40	F	–	Cl	–	–	11	7.959
41	Cl	–	F	–	–	14	7.854
42	Cl	–	Cl	–	–	30	7.523
43*	F	–	–	F	–	130	6.886
44*	Cl	–	–	Cl	–	280	6.553
45*	F	–	–	–	F	95	7.022
46	Cl	–	–	–	Cl	90	7.046
47*	F	–	F	–	F	200	6.699
48*	Cl	–	F	–	Cl	68	7.167
49*	F	F	F	F	F	4,300	5.367
50	–	F	F	–	–	270	6.569
51	–	Cl	F	–	–	140	6.854
52	–	Cl	Cl	–	–	260	6.585
53*						14	7.854
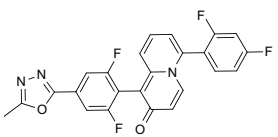
Table 1 (*Continued*)

Compound number	A	B	C	D	E	p38α IC$_{50}$ (nm)	pIC$_{50}$
54						13	7.886

55–70

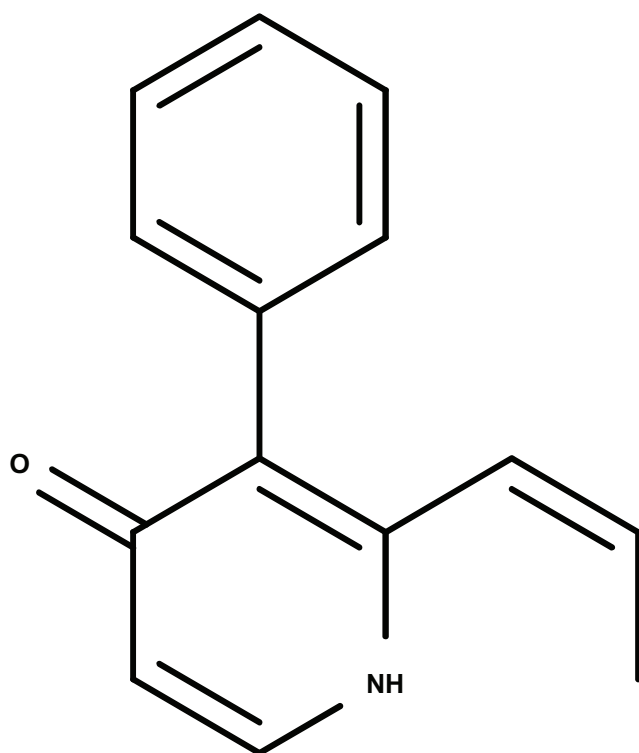| Compound number	R$_1$	R$_2$	p38α IC$_{50}$ (nm)	pIC$_{50}$
55	F	H	17	7.770
56*	F	COOCH$_3$	1.3	8.886
57	F		2.3	8.638
58	F		32	7.495
59	F		9	8.046
60	F		99	7.004
61		COOCH$_3$	0.580	9.237
62			3.3	8.481
63			2.3	8.638
64			5.8	8.237
65			9.9	8.004
66	OCH$_3$	H	8.8	8.056
67	OCH$_3$	COOCH$_3$	0.580	9.237
68	OCH$_3$		1.6	8.775
69	OCH$_3$		1.6	8.796
70	OCH$_3$		0.330	9.481

Note: *Test set compounds.
Abbreviations: MAPK, mitogen activated protein kinase; pIC$_{50}$, the predicted concentration of the compound producing 50% inhibition.

steric and electrostatic interaction fields were calculated using Lennard-Jones and Columbic potentials, respectively, at each lattice intersection. Steric and electrostatic cutoffs were truncated to its default of ±30 kcal/mol, respectively,

and the scale was set to the CoMFA standard. Interaction energies were calculated using a Tripos force field.

The CoMSIA analysis mainly measures five descriptors, ie, steric, electrostatic, hydrophobic, hydrogen bond donor,
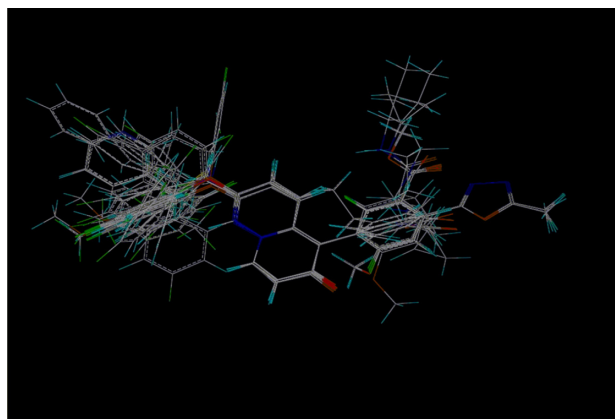
Figure 1 Fragment used as a common structure for aligning database.

was used, in which the CoMFA and CoMSIA descriptors were used as independent variables and pIC$_{50}$ values as the dependent variable. Before proceeding to PLS analysis, the CoMFA and CoMSIA columns were added, and column filtering was set to 2.0 kcal/mol to improve the signal-to-noise ratio and to reduce the time needed for analysis.

The leave-one-out cross-validation method was carried out to check the predictivity of the generated model and to find the optimum number of components leading to high cross-validation (q^2). In this method, one compound is omitted from the dataset and the model is generated using the remaining compounds in the dataset, and the generated model is used further to predict the activity of the omitted compound. Models are considered to be acceptable if they provide a q^2 value >0.5 and $r^2 >0.616$.[15] The cross-validated q^2 was used to generate the optimum number of components and the lowest standard error of prediction. It is generally estimated as:

$$q^2 = 1 - \frac{\Sigma \left(Y_{predicted} - Y_{observed} \right)}{\Sigma \left(Y_{observed} - Y_{mean} \right)} \tag{2}$$

The optimum number of components obtained from the leave-one-out cross-validation method was used further to determine the non-cross-validated r^2 (r^2_{ncv}) and to get the final CoMFA and CoMSIA model. Finally, to check the statistical confidence and robustness of the generated model, bootstrap analysis was performed. This is a method in which n random selections are made from the original set of n objects and is performed several times (100 times were required to obtain good statistical information). In each run, some objects may be excluded from the PLS analysis, whereas others might be included several times. The mean correlation coefficient is represented as bootstrap r^2 (r^2_{bs}).[16–18]

Predictive correlation coefficient

The predictive ability of the generated 3D-QSAR model was found from a test set of 25 compounds. These compounds were aligned to the template and their pIC$_{50}$ values were predicted. The predictive correlation coefficient (r^2_{pred}), based on the test set of compounds, was calculated by the following equation:

$$r^2_{pred} = \frac{(SD - PRESS)}{SD} \tag{3}$$

SD is the sum of the squared deviations between the inhibitory activities of the test set and mean activities of the training set compounds and PRESS is the sum of the squared

Partial least squares analysis and model validation

To derive the 3D-QSAR models, the PLS analysis approach, an extension of multiple regression analysis,

and hydrogen bond acceptor.[12] The region was defined automatically using the probe atom with a charge of +1, a hydrogen bond donor and acceptor property of +1 and hydrophobicity +1, and the attenuation factor (α) was set to its default of 0.3 to smoothen the function, and other parameters were the same as that of the CoMFA field.

Figure 2 Alignment of compounds 1–70 employed for comparative molecular field analysis and comparative molecular similarity indices analysis.

deviations between actual and predicted activity values for each compound in the test set.[19–21]

Results and discussion

To perform the 3D-QSAR analysis, all the compounds were aligned together using fragment as shown in Figure 1, and alignment of the database is reported in Figure 2. To check whether the generated QSAR model is suitable for predicting the activity of unknown compounds, a number of statistical parameters were generated, including the cross-validated correlation coefficient (q^2) by the leave-one-out method, the non-cross-validated correlation coefficient (r^2_{ncv}), standard error of estimate (SEE), significance value (F), and optimum number of components, the average r^2 from a bootstrapping (r^2_{bs}) analysis for 100 runs; the average SEE value from a bootstrapping (SEE$_{bs}$) analysis for 100 runs; cross-validation (r^2_{cv}) by two groups (leave-half-out method); and the predicted correlation coefficient (r^2_{pred}) for the test set compounds.

CoMFA studies

For the CoMFA model, PLS analysis was carried out and the best results were obtained by keeping the column filtering at its default value of 2.0 kcal/mol for both the steric and electrostatic fields. The highest q^2 value was used to find out the optimum number of components with the lowest SEE. PLS analysis was first performed using the leave-one-out method, which showed a high q^2 value of 0.611 with seven components for CoMFA. The non-cross-validated PLS analysis was performed with the same seven components and column filtering was set to off, resulting in $r^2 = 0.973$, $F = 193.933$, and SEE = 0.219. Steric and electrostatic field contributions were 0.580 and 0.420, respectively. All the statistical parameters related to the CoMFA model are given in Table 2, and the reliability of the model was supported with cross-validation and bootstrapping results. The experimental and predicted pIC$_{50}$ values for the training set and test set according to the CoMFA model are given in Tables 3 and 4, respectively, and the distribution is shown in Figure 3.

CoMSIA studies

Because good results were obtained with CoMFA, the same model was used for CoMSIA, and the model was generated using steric, electrostatic, hydrophobic, hydrogen bond acceptor, and hydrogen bond donor fields. The CoMSIA column was first added by creating the region automatically and setting the attenuation factor to its default of 0.3. PLS analysis was first performed using the leave-one-out

Table 2 Summary of CoMFA and CoMSIA results

PLS analysis	CoMFA	CoMSIA
Parameter		
Compounds (n)	45	45
r^2_{LOO} (q^2)	0.611	0.503
ONC	7	5
SEE	0.219	0.564
r^2_{ncv}	0.973	0.815
F value	193.933	34.458
Steric contribution	0.580	0.116
Electrostatic contribution	0.420	0.257
Hydrophobic contribution	–	0.261
H-bond acceptor contribution	–	0.142
H-bond donor contribution	–	0.225
r^2_{bs}	0.981	0.895
SEE$_{bs}$	0.157	0.428
r^2_{cv}	0.595	0.546
Test set r^2 (r^2_{pred})	0.630	0.409
SEP	0.427	0.681

Abbreviations: ONC, optimum number of components; CoMFA, comparative molecular field analysis; SEE, standard error of the estimate; CoMSIA, comparative molecular similarity indices analysis; SEP, standard error of predictability; PLS, partial least squares; q^2, cross-validated correlation coefficient by the leave-one-out method; r^2ncv, the non-cross-validated correlation coefficient; r^2bs, the average r^2 from a bootstrapping analysis for 100 runs; r^2cv, cross validation correlation coefficient by two groups (leave-half-out method); r^2pred, predicted correlation coefficient for the test set compounds.

method, which showed a q^2 value of 0.493 with five components (the optimum component number) for CoMSIA. Non-cross-validated PLS analysis was performed with the same five components and the column filtering set to off, resulting in an $r^2_{ncv} = 0.815$, SEE = 0.564, steric contribution = 0.116, electrostatic contribution = 0.257, hydrophobic contribution = 0.261, H-bond donor contribution = 0.225, and H-bond acceptor contribution = 0.142. All statistical parameters related to the CoMSIA model are shown in Table 2. The statistical quality of the generated model was analyzed further by bootstrapping analysis and by more robust cross-validation using two groups (leave-half-out method) to check the internal reliability within the dataset. On cross-validation by two groups, r^2_{cv} for CoMFA and CoMSIA was found to be 0.595 and 0.546, respectively. Values for bootstrapped r^2_{bs} (the mean r^2 value of bootstrapping analysis) and SEE were 0.981 and 0.157 for CoMFA, respectively, and 0.895 and 0.428 for CoMSIA, respectively, indicating that there was good internal reliability within the dataset. These results show that the 3D-QSAR models generated in this study are relatively steady and retain statistical significance and have high internal predictive ability.

The CoMFA model had a high q^2 value of 0.611 and r^2 (r^2_{pred}) of 0.630 for the test compounds as compared with the CoMSIA model, which had a q^2 value of 0.493 and an r^2 (r^2_{pred}) value of 0.409 for the test compounds. Also, the

Table 3 Experimental and predicted pIC$_{50}$ values and residual values of training set compounds by CoMFA and CoMSIA

Compound number	Experimental values	CoMFA		CoMSIA	
		Predicted	Residual	Predicted	Residual
10	8.328	8.326	0.002	7.648	0.680
12	5.886	5.823	0.063	5.385	0.501
13	6.796	7.025	−0.229	6.418	0.378
14	5.000	4.916	0.084	5.352	−0.352
16	6.143	6.018	0.125	6.986	−0.843
17	8.456	8.294	0.162	8.357	0.099
18	7.699	7.644	0.055	8.010	−0.311
19	6.187	6.116	0.071	5.982	0.205
20	6.319	6.605	−0.286	5.644	0.675
22	8.119	7.577	0.542	7.572	0.547
25	7.036	7.199	−0.163	6.587	0.449
27	5.620	5.393	0.227	6.421	−0.801
28	6.377	6.506	−0.129	6.195	0.182
29	6.620	6.604	0.016	6.304	0.316
30	7.155	6.721	0.434	6.389	0.766
31	5.000	5.178	−0.178	5.804	−0.804
32	5.000	5.015	−0.015	6.063	−1.063
33	7.319	7.297	0.022	6.691	0.628
35	6.585	6.634	−0.049	6.333	0.252
36	5.000	5.118	−0.118	6.112	−1.112
37	5.000	5.041	−0.041	6.547	−1.547
38	7.495	7.763	−0.268	7.542	−0.047
40	7.959	7.556	0.403	7.131	0.828
41	7.854	7.837	0.017	7.220	0.634
42	7.523	7.683	−0.160	7.325	0.198
46	7.046	7.237	−0.191	7.083	−0.037
50	6.569	6.635	−0.066	6.486	0.083
51	6.854	6.801	0.053	6.600	0.254
52	6.585	6.651	−0.066	6.707	−0.122
54	7.886	7.954	−0.068	7.496	0.390
55	7.770	7.772	−0.002	7.417	0.353
57	8.638	8.868	−0.230	8.937	−0.299
58	7.495	7.580	−0.085	7.612	−0.117
59	8.046	7.781	0.265	7.803	0.243
60	7.004	7.102	−0.098	7.599	−0.595
61	9.237	9.112	0.125	9.402	−0.165
62	8.481	8.475	0.006	8.666	−0.185
63	8.638	8.730	−0.092	8.695	−0.057
64	8.237	8.156	0.081	8.159	0.078
65	8.004	8.091	−0.087	8.106	−0.102
66	8.056	8.588	−0.532	8.318	−0.262
67	9.237	8.861	0.376	9.111	0.126
68	8.775	8.919	−0.144	8.564	0.211
69	8.796	8.646	0.150	8.676	0.120
70	9.481	9.463	0.018	9.858	−0.377

Abbreviations: CoMFA, comparative molecular field analysis; CoMSIA, comparative molecular similarity indices analysis; pIC$_{50}$, the predicted concentration of the compound producing 50% inhibition.

standard error of predictability was low for the CoMFA model (0.427) as compared with that for the CoMSIA model (0.681). Therefore, the CoMFA model is more accurate, reliable, and predictive for designing newer analogs. The experimental and predicted pIC$_{50}$ values for the training set and the test set using the CoMSIA model are given in Tables 3 and 4, respectively, and the distribution is shown in Figure 4.

3D-QSAR visualization

The most important characteristic of CoMFA and CoMSIA is that the results are visualized in the form

Table 4 Experimental and predicted pIC$_{50}$ values and residual values of test set compounds by CoMFA and CoMSIA analysis

Compound number	Experimental values	CoMFA		CoMSIA	
		Predicted	Residual	Predicted	Residual
1	8.155	6.754	1.401	5.856	2.299
2	6.495	7.028	−0.533	6.129	0.366
3	6.721	7.107	−0.386	5.715	1.006
4	7.032	6.854	0.178	6.393	0.639
5	6.060	7.320	−1.260	6.981	−0.921
6	6.051	7.437	−1.386	6.182	−0.131
7	6.310	5.522	0.788	5.750	0.560
8	8.495	7.038	1.457	6.625	1.87
9	6.143	6.295	−0.152	5.628	0.515
11	5.000	5.956	−0.956	5.555	−0.555
15	5.886	5.668	0.218	7.328	−1.442
21	5.845	7.277	−1.432	7.414	−1.569
23	7.921	7.094	0.827	6.740	1.181
24	7.357	7.297	0.060	6.944	0.413
26	7.086	7.232	−0.146	6.155	0.931
34	7.102	7.124	−0.022	6.794	0.308
39	7.495	7.622	−0.127	7.889	−0.394
43	6.886	7.824	−0.938	6.765	0.121
44	6.553	7.627	−1.074	6.993	−0.44
45	7.022	7.386	−0.364	6.821	0.201
47	6.699	7.645	−0.946	7.093	−0.394
48	7.167	7.456	−0.289	7.356	−0.189
49	5.367	7.347	−1.980	6.892	−1.525
53	7.854	7.872	−0.018	7.107	0.747
56	8.886	8.133	0.753	8.206	0.680

Abbreviations: CoMFA, comparative molecular field analysis; CoMSIA, comparative molecular similarity indices analysis; pIC$_{50}$, the predicted concentration of the compound producing 50% inhibition.

of three-dimensional coefficient contour maps which are calculated as the variation in molecular fields (the standard deviations and the least squares coefficients (StDev*Coeff) assigned to each grid intersection were contoured within the binding pocket. Further, to visualize the information derived from the 3D-QSAR model, CoMFA and CoMSIA contour maps were generated to identify the regions in three-dimensional space surrounding the molecules and the important regions where changes can be made in these fields which may affect the biological activity and be useful for further optimization of pyridopyridazin-6-ones as p38-α MAPK inhibitors. For better understanding, compound 70 is shown as composed of three regions (Figure 5A–C).
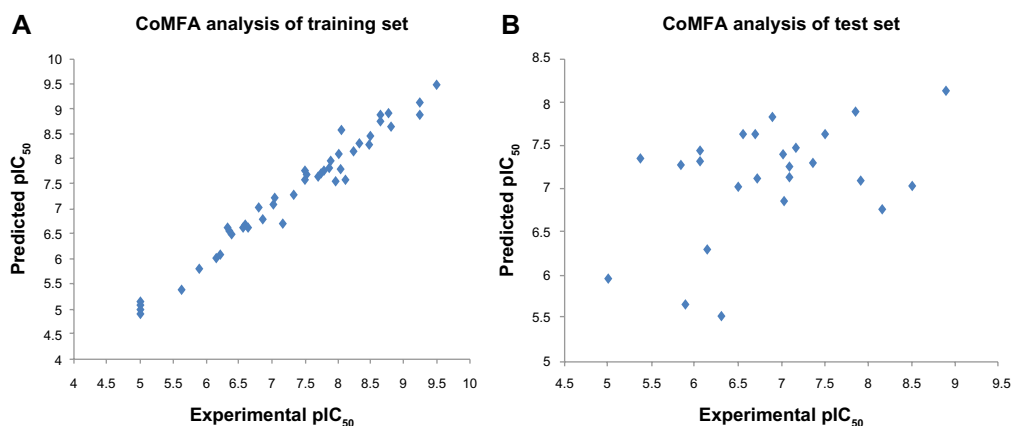
Figure 3 (**A**) Distribution of experimental and predicted pIC$_{50}$ values for training set. (**B**) Distribution of experimental and predicted pIC$_{50}$ values for test set compounds by CoMFA analysis.
Abbreviations: CoMFA, comparative molecular field analysis; pIC$_{50}$, the predicted concentration of the compound producing 50% inhibition.
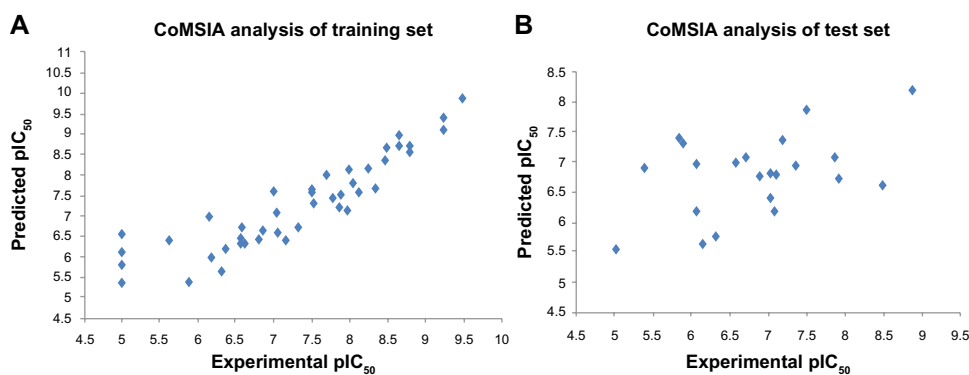
Figure 4 (**A**) Distribution of experimental and predicted pIC_{50} values for training set. (**B**) Distribution of experimental and predicted pIC_{50} values for test set compounds by CoMSIA analysis.
Abbreviations: CoMSIA, comparative molecular similarity indices analysis; pIC_{50}, the predicted concentration of the compound producing 50% inhibition.

CoMFA contour map analysis

To examine the three-dimensional field model generated by CoMFA, the most potent compound in the series, compound 70, was selected, and CoMFA contour maps were generated around it by setting the contour style to solid for visualization of the contour around the ligand, as shown in Figure 6. The steric field contribution is illustrated by green and yellow contour maps. The green areas favor steric bulk, and adding bulky substituents near these areas can improve activity, and yellow areas do not favor steric bulk, so adding bulky substituents near these areas can reduce activity.

In Figure 6A, a big cloud of green contour around region A indicates that introduction of a bulky group in this region is favored. This is evident from the experimental activity values for compounds 1, 8, 10, 17, 22, 23, 40–42, 53, and 70, which have more bulky groups than compounds 2–7, 9, 11–16, 18–21, 24–39, and 43–52. For compounds 1, 8, 10, 17, 22, 23, 40–42, 53, and 70 the bulkier group in region A may impart better activity than compounds 2–7, 9, 11–16, 18–21, 24–39, and 43–52 in which less bulkier groups are present, which may lead to a decrease in activity. Also, the green contour near region C indicates that accommodation of the bulky group is favored in this region. This is evident by comparing the activities of compounds 70 and 69, which have a more bulky group near region C, hence were most potent.

As seen in Figure 6C of the contour map of compound 37, there are no bulkier groups at regions A and C, while a bulky group (–CF_3) is placed in the yellow region, which is not favored for bulky groups. Hence, this leads to a remarkable decrease in the activity of compound 37. The electrostatic field is represented by blue and red contour maps, indicating the regions where electron-donating and electron-withdrawing groups, respectively, are favored.
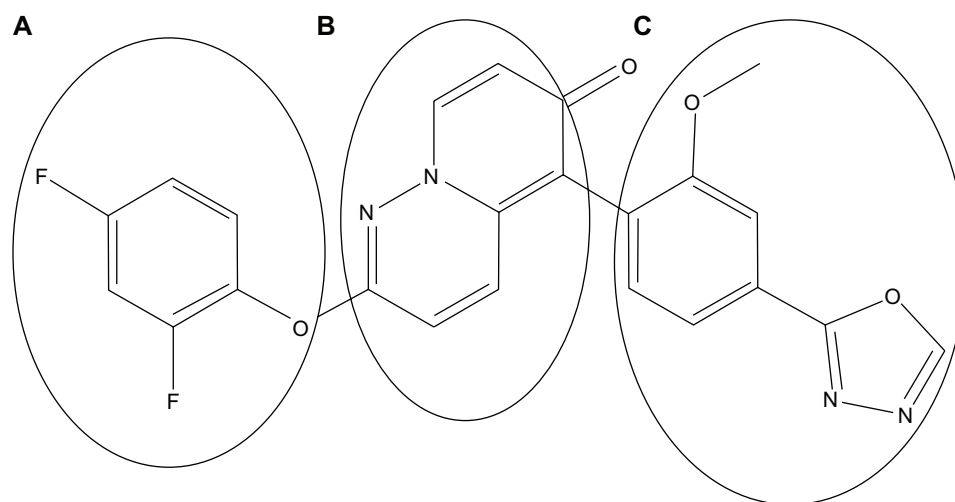
Figure 5 Compound 70 divided into (**A**), (**B**), and (**C**) regions.
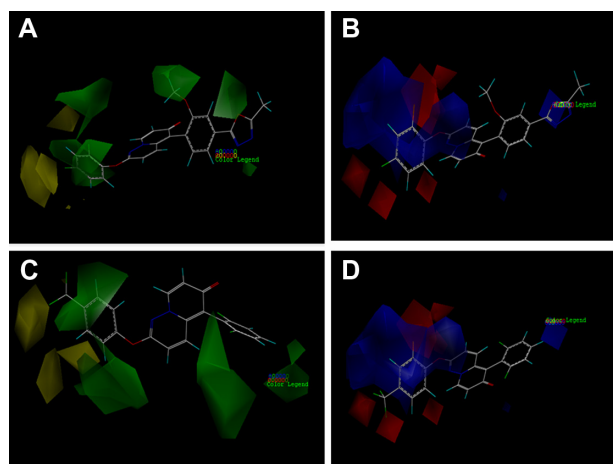
Figure 6 StDev*Coeff contour maps of comparative molecular field analysis showing steric (**A** and **C**) and electrostatic fields (**B** and **D**) mapped with the most active compound in the series, compound 70 (**A** and **B**) and the least potent compound in the series, compound 37 (**C** and **D**).
Notes: Green contours show favorable bulky group substitution at that point while yellow regions show disfavorable bulky group for activity. Red contours indicate negative charge favoring activity, whereas blue contours indicate positive charge favoring activity.
Abbreviation: StDev*Coeff, standard deviations and the least squares coefficients assigned to each grid intersection were contoured within the binding pocket.

Compound 70 was again selected as the reference standard. As seen in Figure 6B, the red contour near region A indicates that electron-withdrawing substituents in this area can increase activity. This is evident from compounds 11, 14, 21, and 70, which can be ranked according to their activity as 70 > 11 > 21 > 14, in which compound 70 has two electron-withdrawing groups in region A, while the others have no electron-withdrawing groups in this region. Hence, compound 70 is the most potent among the series. The blue contour is observed near —O— of region A, suggesting that electron-donating groups outside region A will enhance activity, which is evident from activity of compounds 8, 11, 17, 21, and 70. The activity of compounds 8, 11, 17, 21, and 70, which contain —O, —NH—, —S—, —OCH2, and —CH2—, respectively, can be ranked as 70 > 8 > 17 > 11 > 21. Also, a blue contour is present around the oxadiazole of region C, indicating that electron-donating groups would enhance activity, which is evident from the experimental values of compound 61.

Figure 6A and B, shows a green contour and a red contour near region A, indicating that bulky groups along with electron-withdrawing substituents in this region are favored for activity, which is evident from the most potent compound in the series, compound 70. Compound 37 lacks these bulky substitutions, as shown in Figure 6B, and hence is found to be the least potent.

CoMSIA contour map analysis

Contour maps for steric and electrostatic fields in the CoMSIA model are almost the same as those in the CoMFA model. Few
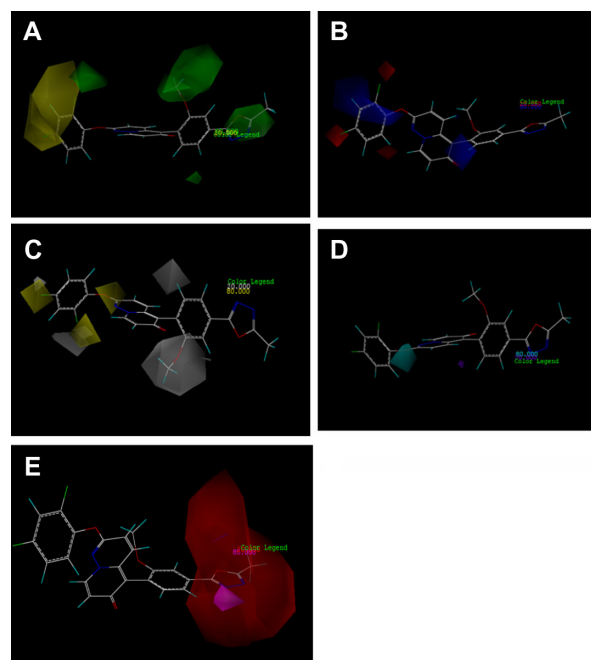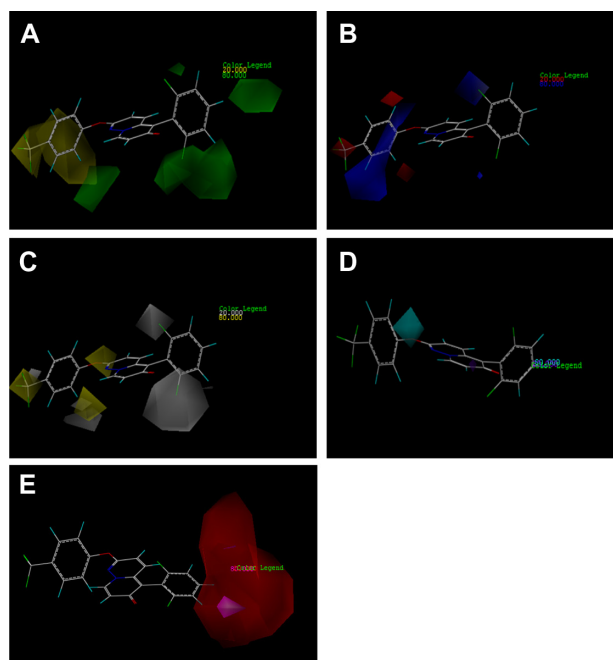

Figure 7 StDev*Coeff contour maps of comparative molecular similarity indices analysis showing (**A**) steric, (**B**) electrostatic, (**C**) hydrophobic, (**D**) hydrogen bond donor, and (**E**) hydrogen bond acceptor fields in combination with compound 70.
Notes: Green contours show favorable bulky group substitution at that point while yellow regions show disfavorable bulky group for activity. Red contours indicate negative charge favoring activity, whereas blue contours indicate positive charge favoring activity. The magenta contour for hydrophobic favored region, gray indicates the hydrophilic favored region. The purple contour for H-bond acceptor group increases activity, cyan indicates the disfavored region; the orange and blue contours represent favored and disfavored hydrogen bond donor groups respectively.
Abbreviation: StDev*Coeff, standard deviations and the least squares coefficients assigned to each grid intersection were contoured within the binding pocket.

more contours are seen for the steric and electrostatic fields which are elaborated here. The green contour seen near the oxadiazole ring of region C in Figure 7A shows that the bulky group in this region is favorable for activity. The oxadiazole ring in compound 70 is mapped in this green contour, but is absent in the least potent compound in the series, compound 37, as seen in Figure 8A. Also, the green contour near the ortho and para position of region A shows that bulky groups are favored in this region, as illustrated in compound 70, which have two fluoro substituents, while compound 37 lacks bulky substituents and has only one —CF3 substituent, leading to a decrease in activity. In Figure 7B, the blue contour near the ortho position of the benzene ring in region C indicates that electron-donating groups in this region favor inhibitory activity. The activity of compound 37 is remarkably decreased because it has electron-withdrawing substituents like fluoro at this position.

The yellow region in the CoMSIA hydrophobic contour plot indicates that hydrophobic substituents in this region enhance inhibitory activity, while the white contour indicates that hydrophilic substituents will improve activity.

Figure 8 StDev*Coeff contour maps of comparative molecular similarity indices analysis showing (**A**) steric, (**B**) electrostatic, (**C**) hydrophobic, (**D**) and hydrogen bond donor, and (**E**) acceptor fields in combination with compound 37.
Notes: Green contours show favorable bulky group substitution at point while yellow regions show disfavorable bulky group for activity. Red contours indicate negative charge favoring activity, whereas blue contours indicate positive charge favoring activity. The magenta contour for hydrophobic favored region, gray indicates the hydrophilic favored region. The purple contour for H-bond acceptor group increases activity, cyan indicates the disfavored region; the orange and blue contours represent favored and disfavored hydrogen bond donor groups respectively.
Abbreviation: StDev*Coeff, standard deviations and the least squares coefficients assigned to each grid intersection were contoured within the binding pocket.

In Figure 7C, the yellow contours of compound 70 observed near the ortho and para position of ring A indicate that bulky substituents are favored in this region. Compound 70 has two bulky substituents in this region, and is the most potent among the series. The least potent compound in the series, compound 37, has fewer bulky substituents in this region, leading to decreased activity. Also, the white contour found near —O— of region C indicates that hydrophilic substituents are favored in this region, which is evident from the contour of compound 37 as seen in Figure 8C which lacks the hydrophilic group and has a bulky —F group, leading to a marked decrease in activity.

In the CoMSIA hydrogen bond donor contour maps, a cyan contour indicates that hydrogen bond donor substituents in this region are favorable for activity, while a purple contour indicates that hydrogen bond donor substituents in this region decrease activity.

In Figure 7D, only one small cyan contour was observed, suggesting that hydrogen bond donor substituents had little influence on activity. The cyan contour was observed near

—O— in region A, indicating that hydrogen bond donor substituents in this region favor activity, which is evident from the experimental activity of compounds 70, 17, and 18. In CoMSIA hydrogen bond acceptor contour maps, a magenta contour indicates that hydrogen bond acceptor substituents in this region are favorable for activity, while a red contour indicates that hydrogen bond acceptor substituents in this region decrease activity.

In Figure 7E, a magenta contour was observed near the 3-N of oxadiazole in region C, meaning that hydrogen bond acceptor substituents in this region enhance activity. A red contour was also observed near the same region, indicating that a bulky substituent in the same region would decrease activity. This is evident from compounds 59, 61, 63, 67, 68, and 69, in which a hydrogen bond acceptor substituent, —C=O, is present and has high potency.

Conclusion

In the present study, CoMFA and CoMSIA were performed using a training set of 45 p38-α MAPK inhibitors. PLS analysis was performed in order to correlate the CoMFA and CoMSIA descriptors with the observed experimental activity. A significant 3D-QSAR model was generated. This model was further validated by cross-validation and bootstrapping, and the results were found to be significant. Further, this optimized model was used for external validation to predict the activity of 25 test set compounds and had good prediction ability, with a high r^2_{pred} observed for the CoMFA model. Our results show that the CoMSIA model generated has a high SEE and that the predictability power was less than that for the CoMFA model. The bulky electron-withdrawing groups were favored in region A at the ortho and para position. Also, hydrogen bond acceptor groups, like —C=O, in region C will increase p38-α MAPK inhibitory activity. Hence, the CoMFA model can be used further to design novel pyridopyridazin-6-ones as p38-α MAPK inhibitors.

Acknowledgments

Disclosure

The authors report no conflicts of interest in this work.

References

1. Aggarwal BB, Shishodia S, Sandur SK, Pandey MK, Sethi G. Inflammation and cancer: how hot is the link? *Biochem Pharmacol*. 2006;72:1605–1621.
2. Badger AM, Bradbeer JN, Votta B, Lee JC, Adams JL, Griswold DE. Pharmacological profile of SB 203580, a selective inhibitor of cytokine suppressive binding protein/p38 kinase, in animal models of arthritis, bone resorption, endotoxin shock and immune function. *J Pharmacol Exp Ther*. 1996;279:1453–1461.
3. Feldmann M, Brennan FM, Maini RN. Role of cytokines in rheumatoid arthritis. *Annu Rev Immunol*. 1992;14:397–440.
4. Foster ML, Halley F, Souness JE. Potential of p38 inhibitors in the treatment of rheumatoid arthritis. *Drug News Perspect*. 2000;13:488–497.
5. Rutgeerts P, D'Haens G, Targan S, et al. Efficacy and safety of retreatment with anti-tumor necrosis factor antibody (infliximab) to maintain remission in Crohn's disease. *Gastroenterology*. 1999;117:761–769.
6. A. Bemis GW, Salituro FG, Duffy JP, Harrington EM, Inventor. Vertex Pharmaceuticals Incorporated, assignee. Inhibitors of p38. United States Patent US6147080. November 14, 2000. B. Cochran J, Galullo V, Bemis GW, Inventor. Vertex Pharmaceuticals Incorporated, assignee. Inhibitors of p38. United States Patent US7919513. April 5, 2011.
7. Dominguez C, Powers DA, Tamayo N. p38 MAP kinase inhibitors: many are made, but few are chosen. *Curr Opin Drug Discov Dev*. 2005;8:421–430.
8. Tynebor RM, Chen M, Natarajan SR, et al. Synthesis and biological activity of pyridopyridazin-6-one p38 MAP kinase inhibitors. Part 1. *Bioorg Med Chem Lett*. 2011;21:411–416.
9. Tynebor RM, Chen M, Natarajan SR, et al. Synthesis and biological activity of pyridopyridazin-6-one p38α MAP kinase inhibitors. Part 2. *Bioorg Med Chem Lett*. 2012;22:5979–5983.
10. Cramer RD, Patterson DE, Bunce JD. Comparative molecular field analysis (CoMFA). 1. Effect of shape on binding of steroids to carrier proteins. *J Am Chem Soc*. 1988;110:5959–5967.
11. Klebe G, Abraham U, Mietzner T. Molecular similarity indices in a comparative analysis (CoMSIA) of drug molecules to correlate and predict their biological activity. *J Med Chem*. 1994;37:4130–4146.
12. Gokhale VM, Kulkarni VM. Comparative molecular field analysis of fungal squalene epoxidase inhibitors. *J Med Chem*. 1999;42:5348–5358.
13. Tripos Associates Inc. SYBYL-X 2.0. St Louis, MO; Tripos Associates Inc; 2012.
14. Clark M, Cramer RD, Van Opdenbosh NJ. Validation of the general purpose Tripos 5.2 force field. *J Comput Chem*. 1989;10:982–1012.
15. Golbraikh A, Tropsha A. Beware of q2! *J Mol Graph Model*. 2002;20:269–276.
16. Kulkarni SS, Kulkarni VM. Three-dimensional quantitative structure activity relationship of interleukin-1β converting enzyme inhibitors: a comparative molecular field analysis study. *J Med Chem*. 1999;42:373–380.
17. Kharkar PS, Desai B, Kulkarni VM, et al. Three-dimensional quantitative structure-activity relationship of 1,4-dihydropyridines as antitubercular agents. *J Med Chem*. 2002;45:4858–4867.
18. Cichero E, Cesarini S, Spallarossa A, Mosti L, Fossa P. Acylthiocarbamates as non-nucleoside HIV-1 reverse transcriptase inhibitors: docking studies and ligand-based CoMFA and CoMSIA analyses. *J Mol Model*. 2005;15:871–884.
19. Haopeng S, Jia Z, Yadong C, et al. Docking study and three-dimensional quantitative structure-activity relationship (3D-QSAR) analyses and novel molecular design of a series of 4-aminoquinazolines as inhibitors of aurora b kinase. *Chin J Chem*. 2011;29:1785–1799.
20. Abedi H, Ebrahimzadeh H, Ghasemi JB. 3D-QSAR, CoMFA, and CoMSIA of new phenyloxazolidinones derivatives as potent HIV-1 protease inhibitors. *Struct Chem*. 2013;24:433–444.
21. ElGamacy MA. 3D-QSAR studies of thiosemicarbazone and thiocarbamoylpyrazoline antiamebics. *Med Chem Res*. 2013;22:415–432.